Saturated fluorescence method for determination of atomic transition probabilities: Application to the Ar I 430.0-nm ($1s_4$-$3p_8$) transition and the lifetime determination of the upper level

A. Hirabayashi, S. Okuda, Y. Nambu, and T. Fujimoto
Department of Engineering Science, Kyoto University, Kyoto 606, Japan
(Received 11 July 1986)

We have developed a new method for determination of atomic transition probabilities based on laser-induced-fluorescence spectroscopy (LIFS). In the method one produces a known population of atoms in the upper level under investigation and relates it to an observed absolute line intensity. We have applied this method to the argon 430.0-nm line ($1s_4$-$3p_8$): In an argon discharge plasma the $1s_5$-level population and spatial distribution are determined by the self-absorption method combined with LIFS under conditions where the $3p_8$-level population is much lower than that of the $1s_5$ level. When intense laser light of 419.1 nm ($1s_5$-$3p_8$) irradiates the plasma and saturates the $3p_8$-level population, the produced $3p_8$-level population and its alignment can be determined from the $1s_5$-level parameters as determined above, by solving the master equation on the basis of broad-line excitation. By comparing the observed absolute fluorescence intensity of the 430.0-nm line with the above population, we have determined the transition probability to be $A=(3.94\pm0.60)\times10^5\ s^{-1}$. We also determined the $3p_8$-level lifetime by LIFS. Several factors which might affect the measurement are discussed. The result is $\tau=127\pm10$ ns.

I. INTRODUCTION

Almost all experimental determinations of atomic transition probabilities and oscillator strengths, except for those for the transitions terminating on the ground state, have been made by using high-pressure arc plasmas. Electron densities and temperatures are determined through plasma diagnostics, and by assuming local thermodynamic equilibrium (LTE) the upper-level populations N_u are calculated. For a given experiment, the observed emission line intensity I_0 is related to N_u and the transition probability A by

$$I_0=\frac{\Omega}{4\pi}h\nu AN_uVa\ , \tag{1}$$

where Ω is the solid angle accepted by the detection system, V is the observed volume, $h\nu$ is the photon energy, and a represents the decrease in radiation intensity due to reabsorption by other atoms (opacity effect). If the absolute sensitivity Q_λ of the detection system is known, the output S of the detector is related to I_0:

$$S=Q_\lambda I_0\ . \tag{2}$$

By combining the observed S and the calculated N_u, we determine A.

In Table I we present an example of the present status of transition probability determinations taking the Ar I 430.0-nm ($1s_4$-$3p_8$) line as an example.[1–13] A great majority of the experiments makes use of arc plasmas, one exception (the plasma jet) being a LTE plasma, the characteristics of which are essentially the same as the arc plasma. As Table I suggests, transition-probability determinations by the above method are accompanied by large experimental errors. They may originate from, e.g., the spatial nonuniformity of the plasma in the axial and radial directions, the determination of the electron density and temperature, the calibration of the absolute sensitivity of the detection system, the determination of the line intensity by measuring on the recorder trace the "area" of the Stark-broadened line which is superposed on a continuum background, and the effect of radiation trapping.

TABLE I. Ar I 430.0-nm line transition probability. Ar: pure argon. H_β: H_β diagnostics.

Author	A ($10^5\ s^{-1}$)	Ar	H_β	Method
Drawin[a]	3.58±20%		○	Arc
Gericke[b]	3.25±15%	○		Arc
Richter[c]	3.1±10%	○		Arc
Popenoe *et al.*[d]	4.11±11%		○	Arc
Chappelle *et al.*[e]	3.14±12%	○		Plasma jet
Wende[f]	3.1±18%	○		Arc
Bues *et al.*[g]	3.1	○		Arc
Wujec *et al.*[h]	3.66±10%		○	Arc
Houwelingen and Kruithof[i]	3.08±8.5%	○		Arc
Nubbemeyer[j]	3.40±5%	○		Arc
Preston[k]	3.72±4%	○		Arc
Baessler and Kock[l]	3.2±7%	○		Arc
Wiese[m]	3.7±5%			Analysis
This work	3.94±15%			LIFS

[a]Reference 1. [h]Reference 8.
[b]Reference 2. [i]Reference 9.
[c]Reference 3. [j]Reference 10.
[d]Reference 4. [k]Reference 11.
[e]Reference 5. [l]Reference 12.
[f]Reference 6. [m]Reference 13.
[g]Reference 7.

Furthermore, there are two problems associated with the use of Eq. (1). The validity criterion for the establishment of LTE was reexamined, and it has been shown that for equilibrium plasmas, which is a class of plasmas including arc plasmas, the validity criterion by Griem[14] is inappropriate. Thus, the critical electron density given by him is lower than the correct value by a factor of 30 for hydrogen and hydrogenic ions.[15] Secondly, Eq. (1) is valid only when the upper-level population density is spatially isotropic; since the high-pressure arc plasma is collision dominated, we assume this to be the case. However, it is reported that excitation anisotropy, or alignment, is detected for the excited-level population in an atmospheric arc plasma.[16] In such a case, the emission radiation has a spatially anisotropic intensity distribution and is polarized. Since we observe the emission in a particular direction with a detector having an anisotropic sensitivity distribution for different polarizations, the observed intensity is not proportional to N_u, and Eq. (1) is no longer valid.

In Sec. II we propose a different method for determination of atomic transition probabilities. This method is free from many of the above sources of experimental error.

Similar problems also exist in the determination of atomic lifetimes. Table II represents the present status for the upper level of the 430.0-nm transition. Here a number of experimental[17–22] and theoretical lifetime values[22–26] are listed, and they scatter over a factor of 3. Each of the experimental methods is accompanied by various sources of experimental error, and proper precautions should be taken to eliminate or to make a correction for them in designing and analyzing the experiment. For instance, the delayed coincidence method is subject to the cascading effect unless the exciting electron energy is just above the excitation threshold of the upper level concerned. Furthermore, this method is not necessarily free from the effect of radiation trapping which may lead to a prolonged lifetime, even when the lower levels of the transitions are excited levels.[21] To make the matter more complicated, in such a case, radiative disalignment of the upper-level population may affect the measured apparent lifetime.[27] The magnetic resonance method (and the Hanle effect method) provides the product of the inverse lifetime and the Landé g factor. Therefore, the accuracy of the g factor limits that of the lifetime. Radiation trapping also affects measurements with these methods.

TABLE II. $3p_8$-level lifetime.

Author	τ (ns)	Method
Experiment		
Klose[a]	166±19	Delayed coincidence
Verolainen and Oscherovich[b]	148±12	Delayed coincidence
Chenevier and Goulet[c]	130±20	Magnetic resonance
Malakhov and Potyomkin[d]	59±6	Delayed coincidence
Erman and Huldt[e]	120±15	High-frequency electron beam
Borge and Campos[f]	165±14	Delayed coincidence
This work	127±10	LIFS
Theory		
Aymar[g]	126	
Gruzdev and Loginov[h]	129	
	134	
Lilly[i]	121	
Katsonis and Drawin[j]	129	
Borge and Campos[f]	129	

[a]Reference 17. [f]Reference 22.
[b]Reference 18. [g]Reference 23.
[c]Reference 19. [h]Reference 24.
[d]Reference 20. [i]Reference 25.
[e]Reference 21. [j]Reference 26.

We have previously proposed a laser-based method for lifetime measurement,[28] and this method has been tested on the neon $2p^5 3p$ levels and the argon $3p^5 4p$ level.[27] The main advantages of this method are (1) it is free from the cascading effect, and (2) since it employs optical excitation, it is easy to control the alignment in the upper-level population and thus to eliminate its effect. In Sec. III we apply our method to the determination of the lifetime of the argon $3p_8$ level.

II. Ar I 430.0-nm ($1s_4$-$3p_8$) LINE TRANSITION PROBABILITY

As noted in Sec. I, Eqs. (1) and (2) are valid only when the excitation is spatially isotropic and the emission radiation is unpolarized. When these conditions are not satisfied these equations should be generalized in order to allow for the effects of excitation anisotropy, or alignment in the present example. The basic idea of the present method of transition probability determination is by using the pulsed laser-induced-fluorescence spectroscopy (LIFS) we calibrate *in situ* the absolute sensitivity Q_λ of our detection system, and we produce by the laser excitation a known number of the upper-level population N_u along with its alignment. We then use the generalized equations of Eqs. (1) and (2) to determine the transition probability.

A. Experimental arrangement

The basic experimental arrangement common to the sensitivity calibration, the transition probability determination, and the lifetime determination has been described in Refs. 29 and 30, and only a brief account is given here. A nitrogen-laser-excited dye laser delivered a light pulse having a width of 5 ns and a repetition rate of 26 pps. This pulse was transmitted through a multimode optical fiber in order to delay the light pulse and to depolarize the laser light. The light was focused, polarized when necessary by a Glan-Thompson prism, and illuminated the discharge plasma of helium, neon, or argon on its axis.

The Pyrex discharge tube had an inner diameter of 5 mm and a length of 3 cm which was defined by reentrant windows. The base pressure was 3.5×10^{-7} torr before high-purity gas was introduced. A dc discharge was run with a cold cathode. Some atoms in a low-lying excited level in the positive column plasma were excited by the laser light to an excited level, and subsequent fluorescence emission was observed along the direction perpendicular to the laser beam through a monochromator (Nikon G-

250, $f/5$, and a linear reciprocal dispersion of 3.4 nm/mm) with the slit parallel to the laser beam. The intensity was measured with a photomultiplier (Hamamatsu R928); to the first and third dynodes an activating gate pulse of about 4 μs was applied, resulting in a supression ratio of 37. The linear response of the photomultiplier was confirmed to hold up to an output current of 20 mA for a pulsed signal of 5-ns duration. The output of the photomultiplier was fed to a boxcar averager (PAR 162 and 163) with a 1-ns gate, which was triggered by the nitrogen-laser pulse. The output of the boxcar was recorded on an X-Y recorder.

B. *In situ* sensitivity calibration

Again, the details of the method are given in Ref. 29. In a helium discharge plasma, we determined the absolute value of the $2\,^1P$-level population by the self-absorption method combined with LIFS (see Sec. II D). Intense laser light of $\lambda=504.8$ nm ($2\,^1P$—$4\,^1S$) illuminated the plasma to excite and saturate the $4\,^1S$-level population. The population N_u was estimated from the $2\,^1P$-level population as determined above, and we calculated the emission intensity I_0 from Eq. (1). By observing the fluorescence light intensity of the 504.8-nm line, we obtained the output current from the photomultiplier. By combining S and I_0, we determined the absolute sensitivity of our detection system $Q_{504.8}$. A similar procedure was followed to obtain the sensitivity at $\lambda=616.4$ nm by using a neon transition ($1s_3$-$2p_2$) In this case, however, the effect of excitation anisotropy was taken into account and the modified versions of Eqs. (1) and (2) were employed. The above results of the *in situ* calibration were found to be smaller by 11% than the calibration based on a calibrated tungsten lamp. Since the relative sensitivity calibration by using the lamp was much more reliable than its absolute value, we shifted our spectral sensitivity curve by 11% downward over the whole range of wavelength. In the present experiment we used another photomultiplier which had a higher sensitivity than that reported in Ref. 29. At the wavelength of 430.0 nm the absolute sensitivity is $Q_{430.0}=(1.53\pm0.15)\times10^4$ A/W.

The relative sensitivities for polarized photons were determined as follows. A magnetic field of 40 G was applied over the plasma in the direction of observation. This precaution was necessary to destroy any polarization of radiation possibly created by the anisotropy of the plasma geometry. We thus obtained unpolarized plasma radiation. By using an analyzing polarizer, we determined the sensitivity ratio for linearly polarized light to be 0.926:1.079 for Q_π:Q_σ, where π denotes the polarization to the direction of the laser beam, σ is to the direction at right angles to it, and $Q_{\pi(\sigma)}$ is the absolute sensitivity. (The choice of the quantization axis is discussed in Sec. II C.) An advantage of the above *in situ* methods is that they include the effect of transmission and reflection at the discharge-tube wall.

C. Alignment

The $3p_8$ level is excited by pulsed laser light of $\lambda=419.1$ nm ($1s_5$-$3p_8$), and we observe the direct fluorescence light at $\lambda=430.0$ nm ($1s_4$-$3p_8$) immediately after laser excitation. Before the laser excitation the $3p_8$-level population is smaller than the $1s_5$ population by several orders of magnitude. Since the abundance of ^{40}Ar is 99.6%, we neglect the hyperfine structure of these lines. The correlation time of our laser light (approximately the reciprocal spectral width of 10^{-11} s corresponding to the width of 0.01 nm) is shorter than the reciprocal spectral width of the atomic 419.1-nm line of 7×10^{-10} s (Doppler width). Therefore, the condition of "broad-line" excitation is satisfied, and the effect of optical coherence between the upper and lower levels is neglected.[30,31] In the present case of unpolarized-light excitation the quantization axis is defined to be along the laser-beam axis. The unpolarized light is regarded as an incoherent superposition of σ_+ and σ_- circularly polarized light and the density matrix of the level population is diagonalized. Figure 1 shows the Kastler diagram of the 419.1-nm line. The $3p_8$ and $1s_5$ levels have total angular momenta of $J=2$. The magnetic substates connected by the lines in Fig. 1 are optically coupled by the unpolarized light. The laser light excites some of the population N of $1s_5$ to $3p_8$. When the intensity is low the upper-substate population is proportional to the transition probability, i.e., the ratio is 2:5:6:5:2 for $m=-2,-1,0,1,2$, respectively; we have a population imbalance or alignment. In the limit of high intensity the $3p_8$-level population is saturated, and the substates populations are $(2/25)N$, $(3/25)N$, $(2/25)N$, $(3/25)N$, and $(2/25)N$. We thus know the absolute population in terms of N as well as the population imbalance or alignment which is different from the low-intensity case. The population and the alignment are treated quantitatively in Sec. II E.

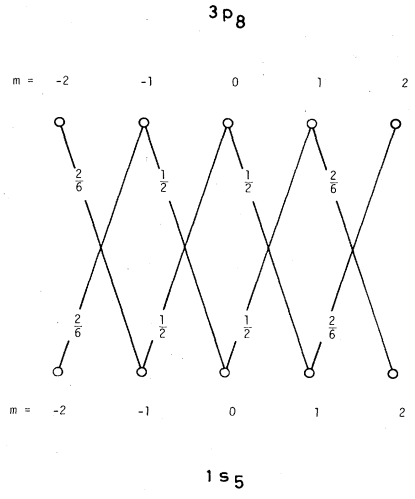

FIG. 1. Kastler diagram of the 419.1-nm transition ($1s_5$-$3p_8$). The laser light is unpolarized: we regard this as incoherent superposition of the $\sigma\pm$ light. Relative transition probabilities for the σ light are indicated.

D. Laser-induced-fluorescence spectroscopy

The laser light was transmitted through a 20-m pure-quartz optical fiber having a core diameter of 0.2 mm. (The doped optical fiber has an appreciable loss for the wavelengths shorter than 450 nm.) With a combination of simple lens and a photographic lens (smc Pentax-A Macro100, $f/2.8$), the image of the fiber core was focused along the axis of the discharge tube. The image at the center of the observed region was calculated to have a diameter of 0.176 mm. To measure the beam profile a slit was placed at the beam waist and the laser beam intensity passing through the slit was measured with a *p-i-n* photodiode as a function of the slit position. An Abel inversion gave the intensity profile; it had a flat top with small wings near the edge. The effective diameter of the flat top was (0.176 ± 0.002) mm. In the following a uniform intensity profile is assumed, and the effect of the wings is included as an uncertainty in the result. Figure 2 illustrates the portion of the plasma which was laser irradiated and observed. The entrance and exit slits of the monochromator had widths of 1 mm and heights of 5 mm. This large width was for the purpose of observing the whole irradiated plasma. The volume was $V=(5.97\pm0.59)\times10^{-10}$ m^3.

The discharge current and the gas pressure were 4 mA and 0.87 torr, respectively. The population of the $1s_5$ level averaged over the tube diameter before laser excitation $\bar{N}$, was determined by the self-absorption method. For this a concave mirror was placed at the side opposite to the monochromator, and we measured the emission intensity of the 696.5-nm ($1s_5$-$2p_2$) line with and without the mirror. From the intensity ratio we determined the lower-level population. Here we adopted the transition probability of 5.92×10^6 s^{-1} on the basis of the lifetime measured by Borge and Campos[22] and the branching ratio by Musiol *et al.*[32] The result was $\bar{N}=1.42\times10^{18}$ m^{-3}. The spatial distribution of the $1s_5$-level population was obtained with the LIFS method and the result is shown in Fig. 3. Since the laser-beam diameter over the observed volume was 0.176—0.754 mm on the axis, we calculated the absolute lower-level population density on the axis before laser excitation as $N=1.64\bar{N}=2.33\times10^{18}$ m^{-3}. The absolute number of lower-level atoms in the observed volume was $NV=(1.39\pm0.16)\times10^9$.

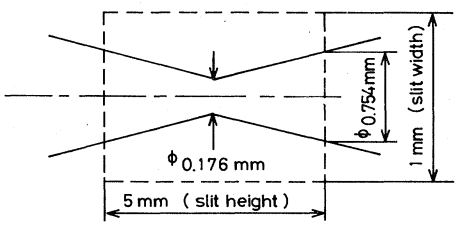

FIG. 2. The side-on view of the part of the plasma which is laser irradiated and observed. The edge of the laser beam is shown with the solid line and the image of the entrance slit with the dashed line.

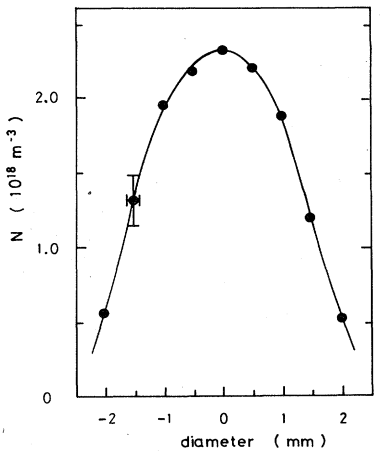

FIG. 3. Population distribution of the $1s_5$ level over the discharge-tube diameter. This is obtained by the self-absorption method combined with LIFS.

E. Saturation characteristics

We calculate here the population and the alignment of the upper level for an arbitrary intensity of illuminating laser light. The master equation for unpolarized broad-line excitation[30] is (see Fig. 1)

$$
\begin{aligned}
\dot{\rho}^u_{22} &= -\Gamma_u\rho^u_{22}+\tfrac{2}{6}\gamma(\rho^l_{11}-\rho^u_{22}) ,\\
\dot{\rho}^u_{11} &= -\Gamma_u\rho^u_{11}+\tfrac{1}{6}\gamma(2\rho^l_{22}+3\rho^l_{00}-5\rho^u_{11}) ,\\
\dot{\rho}^u_{00} &= -\Gamma_u\rho^u_{00}+\gamma(\rho^l_{11}-\rho^u_{00}) ,\\
\dot{\rho}^l_{22} &= -\Gamma_l\rho^l_{22}+\tfrac{2}{6}\gamma(\rho^u_{11}-\rho^l_{22})+\frac{A}{6}(2\rho^u_{11}+4\rho^u_{22}) ,\\
\dot{\rho}^l_{11} &= -\Gamma_l\rho^l_{11}+\tfrac{1}{6}\gamma(2\rho^u_{22}+3\rho^u_{00}-5\rho^l_{11})\\
&\quad +\frac{A}{6}(3\rho^u_{00}+\rho^u_{11}+2\rho^u_{22}) ,\\
\dot{\rho}^l_{00} &= -\Gamma_l\rho^l_{00}+\gamma(\rho^u_{11}-\rho^l_{00})+A\rho^u_{11} ,
\end{aligned}
\tag{3}
$$

with

$$
\gamma=\frac{2\pi}{\hbar^2}I(\lambda)\,|\,d_{ul}\,|^2 , \tag{4}
$$

where $\rho^{u(l)}_{mm}$ is the substate population with the magnetic quantum number m of the upper (lower) level, $\Gamma_{u(l)}$ is the depopulation rate of the upper (lower) level, A and d_{ul} are the spontaneous transition probability[33] and the reduced matrix element of the transition line, respectively, and $I(\lambda)$ is the laser-light density. Since no external field is applied, the off-diagonal elements of the density matrix are absent. It is noted that $\rho^{u(l)}_{-m\,-m}=\rho^{u(l)}_{mm}$. The boundary condition at $t=0$ is

$$
\begin{aligned}
\rho^u_{mm} &= 0 ,\\
\rho^l_{mm} &= N/5 .
\end{aligned}
\tag{5}
$$

For the sake of simplicity, we regard the laser pulse as

having a rectangular shape with a 5-ns width; it is found that the dependence of the solution of Eq. (3) on the laser intensity is insensitive to the choice of the pulse shape or the pulse width. We integrate Eq. (3) and the solution at $t=5$ ns is regarded as corresponding to the peak of the observed fluorescence intensity immediately after the laser excitation. We adopt $\Gamma_u=1.8\times10^7$ s^{-1} (see Sec. III) and $\Gamma_l=0$. The disalignment in the upper and lower levels is not included in the calculation. The error in the final result due to this neglect is estimated to be less than 0.3%.

As shown in Sec. II C and the above, the upper-level population is aligned and the fluorescence emission of the 430.0-nm line is polarized. According to Ref. 30, the π and σ components of the observed fluorescence are described as

$$I_\pi=\tfrac{1}{2}I_0(1+2W_2)\,,\qquad I_\sigma=\tfrac{1}{2}I_0(1-W_2)\,, \tag{6}$$

where I_0 is the intensity that we would observe in the absence of alignment in the upper-level population, Eq. (1), and W_2 is the depolarization coefficient (rank of 2),

$$W_2=(-1)^{J_u-J_f}\left[\frac{3(2J_u+1)}{2}\right]^{1/2}\begin{Bmatrix}J_u & J_u & 2\\ 1 & 1 & J_f\end{Bmatrix}\times\frac{\rho_0^2(J_uJ_u)}{\rho_0^0(J_uJ_u)}\,. \tag{7}$$

Here, J_u and J_f are the total angular momenta of the $3p_8$ and $1s_4$ levels, respectively: $J_u=2$ and $J_f=1$, $\{\ \}$ is the 6-j symbol, and $\rho_0^2(J_uJ_u)$ and $\rho_0^0(J_uJ_u)$ are the irreducible components of the density matrix of the upper level. We note that the coefficient W_2 depends on the laser intensity γ, and Ref. 30 gives its calculation formula for the low- and high-intensity limits. Since we are dealing with the case of $W_2\neq0$, Eq. (2) is modified to include Eq. (6):

$$S=Q_\pi I_\pi+Q_\sigma I_\sigma=Q_\lambda I_0\left[\frac{1+2W_2}{2}\frac{Q_\pi}{Q_\lambda}+\frac{1-W_2}{2}\frac{Q_\sigma}{Q_\lambda}\right]. \tag{8}$$

By using the relation $N_u=\rho_{00}^u+2\rho_{11}^u+2\rho_{22}^u$, we rewrite Eq. (8) as

$$S=Q_\lambda\frac{\Omega}{4\pi}h\nu AN_uF(\gamma)Va\,, \tag{9}$$

where $F(\gamma)$ is the correction factor to Eq. (2) arising from the alignment and the difference in Q_π and Q_σ,

$$F(\gamma)=\frac{3}{2}\left[\frac{\rho_{11}^u+\frac{2}{3}\rho_{00}^u}{2\rho_{22}^u+2\rho_{11}^u+\rho_{00}^u}\frac{Q_\pi}{Q_\lambda}+\frac{\rho_{22}^u+\frac{1}{2}\rho_{11}^u+\frac{1}{6}\rho_{00}^u}{2\rho_{22}^u+2\rho_{11}^u+\rho_{00}^u}\frac{Q_\sigma}{Q_\lambda}\right]. \tag{10}$$

For our conditions $1.03\leq F(\gamma)\leq1.11$, depending on γ.

As suggested by Fig. 2 the laser-light intensity is not uniform along the laser beam. Equation (9) is modified to allow for this variation;

$$S=Q_\lambda\frac{\Omega}{4\pi}h\nu Aa\int_V N_uF(\gamma)dV\,. \tag{11}$$

In the saturation limit the integral in the above equation takes the value of $0.489NV$.

By using a stack of calibrated neutral-density filters, we attenuated the incident laser-light intensity and measured S for the 430.0-nm emission. (Some of the neutral-density filters showed nonlinear transmission, due to the bleaching effect, and they were discarded.) The results are shown in Fig. 4. The effect of superradiance was not observed throughout the measurement (see Appendix for details). The saturation curve or the γ dependence of the integral in Eq. (11) was fitted to the experimental results by adjusting the curve vertically and horizontally. This was necessary since the laser-light intensity was measured only relatively in this experiment. The result of the fitting is also shown in Fig. 4. The absolute value of γ shown in Fig. 4 is for the center of the observed region. The output current of the detection system was obtained to be $(4.60\pm0.04)\times10^{-3}$ A in the saturation limit.

F. Result

For our experimental conditions $\Omega/4\pi=2.48\times10^{-3}$; the correction factor a was estimated from the amount of absorption of radiation emitted at the tube axis on its way to the tube wall: $a=0.98$. By combining the quantities in Eq. (11) we determined the transition probability of the 430.0-nm line as $A=3.94\times10^5$ s^{-1}. Uncertainties accompanying determinations of S, N_uV, and Q_λ are, respectively, 0.9%, 11%, and 10%. Thus, the total uncertainty is 15%:

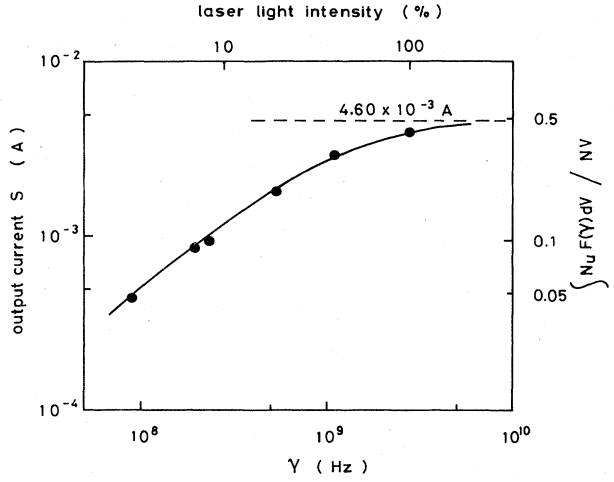

FIG. 4. The output current for the observed fluorescence intensity as a function of the laser-light intensity: Experimental data are fitted to the theoretical curve [see Eq. (11)]. In the saturation limit of the $3p_8$-level population, $\int N_uF(\gamma)dV=0.489NV$ and we obtain the output current of $(4.60\pm0.04)\times10^{-3}$ A.

$A = (3.94 \pm 0.59) \times 10^5\ s^{-1}$.

Table I shows the comparison with other data. Our result is in agreement with Wiese[13] within the error limits.

G. Concluding remarks

We have proposed a laser-based method for determinations of atomic transition probabilities. In this method it is necessary that the following conditions are satisfied:

1. Broad-line excitation.
2. $\gamma \gtrsim \Gamma_u$ (quasisaturation).
3. Superradiance does not take place.

For the methods to confirm these conditions, one is referred to, for example, Ref. 30 and the Appendix of this paper. In the present measurement, the effect of disalignment can be neglected, as described in Sec. II E. When this effect is appreciable, the master equation (3) should be modified to take this into account. The uncertainty of the obtained result is strongly dependent on the laser power through the observed volume. This is because a larger radius of the exciting beam from a higher power laser leads to a smaller uncertainty in defining the volume V. A similar argument also holds for the *in situ* calibration of the detection system (Sec. II B). In the present measurement, the low power of our laser results in a large uncertainty of 15%. If the power had been higher by 2 orders of magnitude, the uncertainty would have been less than 5%.

III. LIFETIME OF THE ARGON $3p_8$ LEVEL

For measurement of the lifetime of the $3p_8$ level, an argon positive column plasma was used as in Sec. II. In this case the discharge current and the gas pressure were 2 mA and 0.09–2 torr, respectively. Before illuminating the plasma the laser light was linearly polarized with a Glan-Thompson prism, where the polarization direction was at an angle of 55° with respect to the direction of observation (magic-angle excitation). The laser beam had a diameter of 1.2 mm at the plasma. A magnetic field of about 40 G was applied over the plasma in the direction of observation; the half Larmor period of about 4 ns was shorter than the time resolution of our detection system of about 5 ns. This combination was necessary to eliminate the alignment effect of the upper level on the decay measurement of the fluorescence intensity. Otherwise, the observed decay would be different from the decay of the population.[28]

The decay rate of the direct fluorescence intensity of the 430.0-nm line ($1s_4$-$3p_8$), or the total depopulation rate of the $3p_8$ level, was measured. The aperture delay range of the boxcar averager was 200 ns, and the time base was calibrated absolutely by using the time-of-flight method of the laser pulse over 16.3 m. Figure 5 shows the observed decay rate as a function of the atom density. The experimental data were fitted to a straight line by the least-squares method as shown in Fig. 5. From the intercept at the low-density limit, the radiative decay rate of the $3p_8$ level was determined as $(7.9 \pm 0.3) \times 10^6\ s^{-1}$, or the neutral lifetime (127 ± 5) ns.

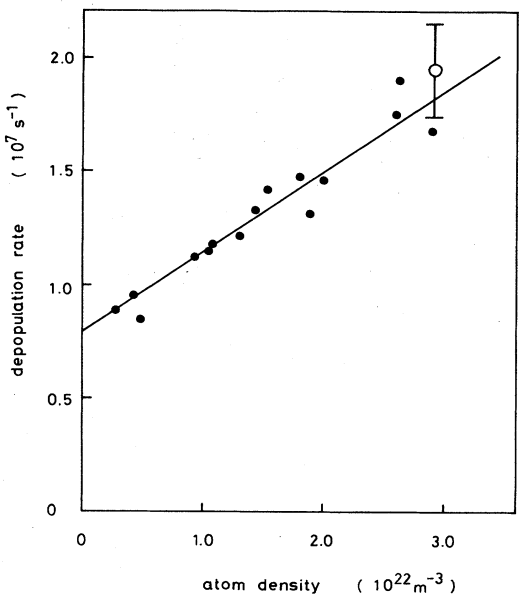

FIG. 5. The depopulation rate of the $3p_8$ level as a function of atom density. The experimental points (●) are fitted to a straight line by the least-squares method: $3.55 \times 10^{-16} N\ (m^3) + 7.90 \times 10^6\ s^{-1}$. The reciprocal of the intercept at the low density limit gives the lifetime of 127 ns. The data point (○) is obtained during the course of the transition probability measurement (see Appendix).

Several factors which might have affected our determination of the lifetime had to be examined. (1) The effect of radiation trapping is examined on the three lines of 419.1 nm ($1s_5$-$3p_8$), 430.0 nm ($1s_4$-$3p_8$), and 462.8 nm ($1s_2$-$3p_8$). Among them, only the 419.1-nm line can have an appreciable effect, since only this line has a metastable lower level. By the same method as in Sec. II D, we determined the population of the $1s_5$ level. The optical thickness of the 419.1-nm line at the line center is calculated to be less than 0.04 under our experimental conditions. For the 430.0- and 462.8-nm lines the optical thickness is much smaller. These small values are due to the fact that these $1s_j$-$3p_8$ transitions are responsible for only a small portion of the radiative decay rate of the upper-level population, about 6%. Thus, the effect of radiation trapping is neglected. (2) Superradiance did not take place. Details are given in the Appendix. (3) A part of the laser-excited population of the $3p_8$ level is collisionally transferred to other $3p_k$ levels and further transferred back to the original level (backtransfer). We neglect this effect, and this is justified as follows. In the case of the neon $2p_3$ level we found that the effect of backtransfer decreased the apparent depopulation rate of the upper level by 9% at a gas pressure of 0.79 torr.[27] By using the appropriate transfer rates in this neon case we made a computer simulation and this was applied to the argon case based on the three-level model. We found that the backtransfer affects only the collisional depopulation rate (the slope in Fig. 5) and

that the maximum error due to its neglect in the lifetime is 3% under the conditions of Fig. 5. Furthermore, the argon $3p_8$ level is expected to be subject to associative ionization; the ionization potential of this level is 1.25 eV and the potential depth of Ar_2^+ molecular ion is 1.30 eV.[34] This assumption is supported by a microwave experiment, where we applied the microwave-cavity resonance method[35] to observe a temporal development of electron density of the plasma following the laser excitation, and we obtained an appreciable increase in electron density. Thus, we conclude that a large portion of the depopulation is carried by associative ionization and the population is lost from the $3p^5 5p$ configuration levels. We estimate the experimental uncertainty due to the neglect of the backtransfer to be 1%. (4) The effect of electron collisions is neglected. This is justified by the fact that the depopulation rate does not change when the discharge current is increased by an order of magnitude.

From the above consideration we estimated the experimental uncertainty. The final result for the lifetime of the $3p_8$ level is (127 ± 10) ns. Table II shows the comparison with other data. Our result agrees with those of Chenevier and Goulet[19] and Erman and Huldt,[21] although the latter experiment needs critical reexamination.[27] The fact that the delayed coincidence experiments, with one exception, give rather large lifetimes suggests that cascading from higher levels affects these lifetime determinations. The theoretical data show almost the same value and agree with the present result.

ACKNOWLEDGMENTS

The authors are grateful to Dr. W. L. Wiese for his stimulating discussion on the lifetime problem of the argon atoms. They wish to thank Mr. K. Ono of Sumitomo Electric Co. for providing us with the pure-quartz optical fiber and Mr. Kojima and Mr. Miyazaki of Asahi Kogaku Co. for lending us the macro lens and computing the diameter of the focused image of the fiber core. They also acknowledge Y. Uetani and M. Hasuo for their assistance in this work and Dr. G. Dunn for his help in completing the manuscript. This work was supported by Grant-in-Aid for Fusion Research from the Ministry of Education, Science and Culture.

APPENDIX: SUPERRADIANCE

When a group of atoms is excited by laser radiation, population inversion may be produced on a transition which originates from the upper level. If the population difference exceeds the threshold value, the excited atoms may start to radiate very strongly to a particular direction (in our case, the discharge-tube axis). This phenomenon is called "superradiance" and is due to the spontaneous phase locking of atomic dipoles. For a nondegenerate two-level system, the threshold population density for superradiance is[36]

$$N_{\rm th}=8\Delta\omega_D/l\lambda^2 A\ , \qquad \text{(A1)}$$

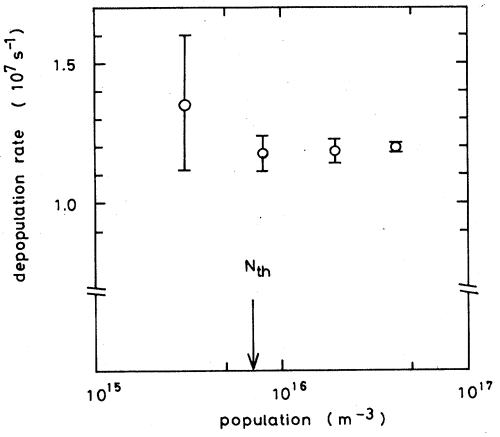

FIG. 6. The depopulation rates of the $3p_8$ level against the population of this level. $N_{\rm th}$ is the estimated threshold population for superradiance. No appreciable increase in depopulation with increasing population density over $N_{\rm th}$ is seen.

where $\Delta\omega_D$ is the Doppler width, l is the length of the medium, and λ is the wavelength of the line. If superradiance took place to a line originating from the $3p_8$ level, the population of this level would have been lost within a short time; as its result, we would have obtained a shorter lifetime and a smaller transition probability. Thus, superradiance should be avoided in our measurements.

In this present case the $3p^5 5p$ configuration level $3p_8$ has three transition arrays: $4s$-$5p$, $5s$-$5p$, and $3d$-$5p$. As Eq. (A1) suggests, the $5s$-$5p$ transitions have the lowest threshold value and, among them, the 2.98-μm line ($2s_4$-$3p_8$) has the smallest value of $N_{\rm th}$: 7×10^{15} m^{-3} for $l=3$ cm, where the transition probability of this line is adopted from Ref. 26.

In the lifetime measurement, the maximum population density immediately after the laser excitation N_u was about 4×10^{16} m^{-3}, apparently above the threshold. Therefore, it was probable that the superradiance took place. Figure 6 shows an example of the measured depopulation rate as a function of N_u (the discharge current is 2 mA for the pressure of 0.4 torr). The population density N_u was changed by attenuating the laser-light intensity and the depopulation rate was measured. (The data shown in Fig. 5 were obtained at the maximum laser intensity.) Figure 6 shows no appreciable increase in the depopulation rate with increasing N_u over the threshold value $N_{\rm th}$ indicated with the arrow. We thus conclude that no superradiance has taken place.

In the transition-probability measurement, the maximum population N_u was 1.12×10^{18} m^{-3}. For this condition, we measured the depopulation rate of the $3p_8$ level (0.87 torr, 4 mA) as $(1.97\times0.20)\times10^7$ s^{-1}. This is plotted in Fig. 5 and shows good agreement with the depopulation rate obtained in the lifetime measurement. Thus we conclude that no superradiance has taken place, too, in this case. The good agreement in Fig. 4 between the experiment and the calculation supports our conclusion.

[1]H.-W. Drawin, Z. Phys. **146**, 295 (1956).
[2]W. E. Gericke, Z. Astrophys. **53**, 68 (1961).
[3]J. Richter, Z. Astrophys. **61**, 57 (1965).
[4]C. H. Popenoe and J. B. Shumaker, Jr., J. Res. Nat. Bar. Stand. Sect. A **69**, 495 (1965).
[5]J. Chapelle, A. Sy, F. Cabannes, and J. Blandin, J. Quant. Spectrosc. Radiat. Transfer **8**, 1201 (1968).
[6]B. Wende, Z. Phys. **213**, 341 (1968).
[7]I. Bues, T. Haag and J. Richter, Astron. Astrophys. **2**, 249 (1969).
[8]T. Wujec, Acta Phys. Polon. **36**, 269 (1969).
[9]D. van Houwelingen and A. A. Kruithof, J. Quant. Spectrosc. Radiat. Transfer **11**, 1235 (1971).
[10]H. Nubbemeyer. J. Quant. Spectrosc. Radiat. Transfer **16**, 395 (1976).
[11]R. C. Preston, J. Quant. Spectrosc. Radiat. Transfer **18**, 337 (1977).
[12]P. Baessler and M. Kock, J. Phys. B **13**, 1351 (1980).
[13]W. L. Wiese, in *The Physics of Ionized Gases,* edited by G. Pichler (Zagreb University, Yugoslavia, 1982), p. 435.
[14]H. R. Griem, *Plasma Spectroscopy* (McGraw-Hill, New York, 1964), p. 129.
[15]T. Fujimoto, J. Phys. Soc. Jpn. **54**, 2905 (1985).
[16]L. Ya. Margolin, N. Ya. Polynovskaya, L. N. Pyatnitskii, R. Sh. Timergaliev, and S. A. Edel'man, Teplofiz. Vys. Temp. **22**, 193 (1984) [High Temp. (USSR) **22**, 149 (1984)].
[17]J. Z. Klose, J. Opt. Soc. Am. **58**, 1509 (1968).
[18]Ya. F. Verolainen and A. L. Osherovich, Opt. Spektrosk. **25**, 866 (1968) [Opt. Spectrosc. (USSR) **25**, 258 (1968)].
[19]M. Chenevier and G. Goulet, J. Phys. (Paris) Colloq. **30**, C1-84 (1969).
[20]Yu. I. Malakhov and V. G. Potyomkin, Opt. Spektrosk. **32**, 245 (1972) [Opt. Spectrosc. (USSR) **32**, 129 (1972)].
[21]P. Erman and S. Huldt, Phys. Scr. **17**, 473 (1978).
[22]M. J. G. Borge and J. Campos, Physica **119C**, 359 (1983).
[23]M. Aymar, Physica **57**, 178 (1972).
[24]P. F. Gruzdev and A. V. Loginov, Opt. Spektrosk. **38**, 411 (1975) [Opt. Spectrosc. (USSR) **38**, 234 (1975)].
[25]R. A. Lilly, J. Opt. Soc. Am. **66**, 245 (1976).
[26]K. Katsonis and H. W. Drawin, J. Quant. Spectrosc. Radiat. Transfer **23**, 1 (1980).
[27]T. Fujimoto, C. Goto, Y. Uetani, and K. Fukuda, Phys. Scr. **28**, 617 (1983).
[28]T. Fujimoto, C. Goto, and K. Fukuda, Phys. Scr. **26**, 443 (1982).
[29]A. Hirabayashi, S. Okuda, Y. Nambu, and T. Fujimoto, Appl. Spectrosc. **40**, 841 (1986).
[30]A. Hirabayashi, Y. Nambu, and T. Fujimoto, Jpn. J. Appl. Phys. **25**, 1563 (1986).
[31]C. Cohen-Tannoudji, *Frontiers in Laser Spectroscopy* (North-Holland, Amsterdam, 1977).
[32]K. Musiol, D. W. Jones, and W. L. Wiese, J. Quant. Spectrosc. Radiat. Transfer **29**, 321 (1983).
[33]W. L. Wiese, M. W. Smith, and B. M. Glenon, *Atomic Transition Probabilities,* U.S. National Bureau of Standards National Standard Reference Data Series—4 (U.S. Government Printing Office, Washington D.C., 1966), Vol. 1.
[34]K. P. Huber and G. Herzberg, *Constants of Diatomic Molecules* (Van Nostrand Reinhold, New York, 1979), p. 33.
[35]Y. Uetani and T. Fujimoto, Opt. Commun. **49**, 258 (1984).
[36]J. C. MacGillivray and M. S. Feld, Phys. A **14**, 1169 (1976).